Monthly Notices of the ROYAL ASTRONOMICAL SOCIETY

MNRAS **497,** 5550–5559 (2020) doi:10.1093/mnras/staa2183

Meteors with extreme beginning heights from observations with high-sensitivity super-isocon TV systems

P.M. Kozak[1,2]★ and J. Watanabe[2]

[1]*Astronomical Observatory, Taras Shevchenko National University of Kyiv, Kyiv UA-04053, Ukraine*
[2]*National Astronomical Observatory of Japan, Mitaka, Tokyo 181–8588, Japan*

Accepted 2020 July 17. Received 2020 July 17; in original form 2019 December 3

ABSTRACT

Meteors with extremely high altitudes are considered. Parameters of seven meteors having anomalous beginning heights recorded with highly sensitive super-Isocon TV systems are presented. One 1993 Perseid meteor, one 2001 sporadic meteor and five meteors from the 2002 Leonid storm had beginning heights in the range 135–145 km. The sporadic meteor is used to demonstrate the methods of data processing and observation precision results. The original TV meteor images, photometric calibration curves and meteor light curve are shown. Light curves are shown for the Leonid shower meteors as well. Based on the sporadic meteor and the 2002 Leonid shower meteor data, mass-loss curves were calculated as functions of height and time: the maximum rates of mass loss were 0.14 and 0.20 g s^{-1}, respectively. Using the classic equation for partially isothermal stone particle heating, the detected beginning heights of most meteors considered (136–135 km) are shown to possibly be related to blowing the molten layer off from a meteoroid surface and most segments of the light curves (below 124 km) show intensive evaporation. For some Leonid meteors, appearing higher than 145–140 km, energy exchange of atmosphere molecules and atoms with the 'cold' meteoroid surface can also be assumed. Another possible explanation lies in the low melting temperature of 1500–1600 K for Leonid meteors.

Key words: meteorites, meteors, meteoroids.

1 INTRODUCTION

At present, the Meteor Data Center of the International Astronomical Union (MDC IAU) includes 7873 photographic meteors and 110 581 video meteors (mainly kinematic parameters, including orbital elements), with the video-meteor database continually being widened (Jopek & Kaňuchová 2017). Recently, among all the various meteors detected with TV and video cameras, observers have spotted a number of meteors with some pronounced features or anomalies in their behaviour, kinematic or photometric characteristics (Koten et al. 2019). As an example, we can quote the intriguing ultrashort outbursts of activity in some meteor showers, which ensue from the cluster structure of meteor streams. Thus, Kinoshita, Maruyama & Sagayama (1999) discussed the detection of 100–150 meteors in 2 seconds, while Watanabe et al. (2003) reported 15 meteors in 4 seconds and 38 meteors in 2 seconds in the Leonid stream. Recent observations (Koten at al. 2017) of September ε- Perseids (SPE) showed a cluster consisting of eight small particles, which produced faint meteors that followed a bright bolide while they were observed for less than 2 seconds. Another interesting phenomenon is Earth-atmosphere-grazing meteors. In spite of the fact that such meteors do exist, only a few instances of their registration are known. These are as follows: a bright bolide of –15 to –18 mag over the USA and Canada in 1972 August (Ceplecha 1994); a bolide of –6 mag over the Czech Republic and Poland in 1990 October (Borovička & Ceplecha 1992); a bolide of –8 mag over Japan in 2006 March (Abe et al. 2006); a meteor of –4 mag over Spain in 2012 June (Madiedo et al. 2016); a low-light meteor of +3 mag detected with a high-sensitivity super-isocon TV system in 2003 September over Ukraine (Kozak & Watanabe 2017). Another captivating and rather rare photometric anomaly in meteor development is the bimodal light curve, when, after reaching maximum luminosity, a meteor sharply decreases its luminosity or disappears completely and then develops again (Kozak, Watanabe & Sato 2014; Roberts et al. 2014). In addition to the above-mentioned photometric anomalies, there are a number of others, namely diffuse (nebula) structure of a meteor at the beginning of its trajectory. Such meteors are often registered at extremely high altitudes – see, e.g. Spurny et al. (2000a) – and sometimes at classic ones (Kozak 2019). A bright meteor of –3 mag from the Leonid shower recorded with a 1000 frames per second (fps) high-speed camera had an anomalous shape of its coma, several hundred metres in size and visually resembling a shock wave (Stenbaek-Nielsen & Jenniskens 2004). LeBlanc et al. (2000) and Taylor et al. (2000), relying on video observations, concluded that some meteors from the Leonid shower have transverse luminous jets 0.5–2 km long.

One of the most thought-provoking anomalies in meteor evolution is their occasional appearance at extremely high altitudes. The classic theory of meteor evolution relates the beginning of meteor radiation to intensive evaporation and mass loss (ablation), which must start at altitudes not exceeding 120–125 km, depending on meteoroid density, initial mass, velocity and the entrance-to-atmosphere angle. Nevertheless, in MDC IAU (Jopek & Kaňuchová 2017) one can find six photographic meteors with beginning altitudes of 130–135 km,

★ E-mail: kpm@univ.kiev.ua

© 2020 The Author(s)
Published by Oxford University Press on behalf of the Royal Astronomical Society

Downloaded from https://academic.oup.com/mnras/article/497/4/5550/5900409 by guest on 20 April 2024

with one even exceeding 138 km. The advent of observational TV and later video systems equipped by brightness amplifiers confidently demonstrated possible meteor appearance at altitudes equal to and even exceeding 130 km. Probably, the first TV meteor chronologically that definitely exceeded 130 km was registered in Kyiv during observations of the 1993 Perseid meteor shower. Its beginning height was 136.84 ± 0.12 km. The meteor was studied very meticulously and details published in Hajdukova et al. (1995); later it was included in the catalogue (Kruchinenko et al. 1997). Nevertheless, this meteor has remained little known, probably due to the fact that its beginning height did not exceed the theoretical limit significantly.

The most famous work in this field is that of Japanese observers Fujiwara et al. (1998), in which they describe observations, using sensitive video cameras, of two bright meteors of the Leonid shower in 1995 and 1996. The meteors had absolute magnitudes of –7 and –4 mag and beginning heights approximately equal to 160 km. The velocities in both cases were typical for Leonid shower meteors: 72.1 and 71.3 km s^{-1}. It should be noted that, on the photo films (photo observations were carried out simultaneously), the meteors become visible only at classic altitudes. The authors try to attribute this fact to either markedly higher integral sensitivity of the video cameras than the photographic ones or their sensitivity in the near-infrared region of spectrum up to 900 nm, where the photographic camera is rather insensitive.

Later, the detection of bright meteors at altitudes exceeding 130 km became relatively commonplace. Thus, according to Betlem et al. (1999), during the Dutch expedition to China in 1998 for Leonid observations (1998 Sino-Dutch Leonid Expedition), one bolide (among 75 meteors) of –13 mag with initial velocity 71.8 km s^{-1} was detected with the help of a photographic camera at an altitude of 134.8 km. In parallel with the photographic observations of the Dutch–China group, Czech scientists (Spurny et al. 2000b) carried out video observations with an all-sky camera equipped with an amplifier, where the limiting astronomical magnitude determined by stars (stellar magnitude) was +4 mag. Similarly to Fujiwara et al. (1998), all meteors were video-recorded at altitudes well above those registered by photo cameras. Because the meteor trajectories were calculated by photographic images, the beginning heights of video meteors were calculated by extrapolation, while the meteoroid trajectories were considered to be straight lines. Thus, Spurny et al. (2000b) estimated the beginning heights for 12 bolides of the Leonid shower to be in the range 145–200 km; moreover, a correlation between beginning heights and initial masses of meteors was found. The same 1998 Leonid shower was observed by a Canadian group (Campbell et al. 2000) in Mongolia. They detected only three meteors at altitudes above 130 km, namely 137.96, 144.43 and 130.96 km, with the beginning heights of most meteors being within the confines of 120–90 km.

Quite a number of meteors at extraordinary heights were registered later by Czech researchers; these were not quite as fast as the Leonids. According to Koten et al. (2001), two η-Aquariids (ETA) were detected at altitudes of 150.2 km and 133.8 km, one Perseid – at 149.0 km and one Lyrid (velocity 45.3 km s^{-1}) at 136.8 km. Gährken & Michelberger (2003) reported details of one Leonid at 174 ± 8 km observed on 2002 November 11. Kozak et al. (2007) showed preliminary processed results of the Leonid storm on 2002 November 18/19, where several meteors at altitudes above 135 km were detected; these will be discussed in detail below. During the Orionid meteor shower observations on 2012 October 18/19 (Olech et al. 2013), a bright bolide of –14.7 mag at a height of 168 ± 0.6 km was registered by the Polish Bolide Network. The luminosity of the meteor at the beginning of the trajectory was 1.5 ± 1.0 mag. On 2012 August 12, the Czech Bolide Automatic Observatory recorded a bright Perseid meteor of almost –10 mag, with a beginning height of 170 km (Spurný et al. 2014). The bolide was detected by many cameras, including spectral instrumentation; however, above 130 km only emission of O, N and N_2 was observed.

During the last few decades, double-station observations of meteors with hypersensitive super-isocon TV systems have been performed at the Astronomical Observatory of Taras Shevchenko National University of Kyiv, Ukraine. Despite many technical weaknesses (mainly sharp geometrical and photometric distortion, the dependence of the working mode on many adjustments, etc.), these relatively old-fashioned television transmitting tubes are extremely sensitive to low light fluxes. They allow observation of stars up to +8 and +10 mag using such lenses as Jupiter-3 ($f = 50$ mm, $f/1.5$) and Helios-40 ($f = 85$ mm, $f/1.5$), respectively. Since the main objective of classic kinematic processing of meteor observations was, as a rule, to determine as accurately as possible the meteoroid trajectory parameters and orbital elements, the focus in internal measurements was given to the accuracy of the meteor head position determination in each frame. To achieve this, however, it seemed advisable to drop the points with the faintest images of a meteor that are realized in the first and last frames and points with oversaturated images of a meteor that are realized at its maximum luminosity, i.e. those points where it is difficult to determine meteor position. It is obvious that the meteor height, as a kinematic parameter, in such selected frames was determined reliably, but it did not correspond to the actual height of meteor occurrence. Due to the sensitivity of our TV systems, we decided to remeasure the results of some of our observations, focusing primarily on the first frames, where the appearance of a meteor could have been missed. The selection of meteors for reprocessing and the preliminary processing results has been summarized in Kozak (2017). Here we present the final reprocessing results, including details of internal measurements in TV frames, meteor light curves and a comparative analysis of the results obtained.

2 DATA ANALYSIS OF METEOR OBSERVATIONS OBTAINED WITH HIGH-SENSITIVITY SUPER-ISOCON TV SYSTEMS

2.1 Selected observations, equipment and processing methods

For the reprocessing of double-station meteor observations obtained with super-isocon TV cameras, we have selected two mini-catalogues of sporadic meteors observed around the autumn equinoxes of 2001 (18 meteors) and 2003 (80 meteors), as published in Kozak, Rozhilo & Taranukha (2012) and Kozak et al. (2011), respectively, and a mini-catalogue with the results of preliminary processing of 28 meteors from the 2002 Leonid storm (Kozak et al. 2007). In addition, a catalogue of Perseids 1991–1993 (57 meteors) published in Kruchinenko et al. (1997) underwent revision. All observations were carried out at observational stations of the Astronomical Observatory of Taras Shevchenko National University of Kyiv, located at a basic distance of 54 km. In all cases, meteors with beginning altitudes exceeding, according to our previous calculations, 130 km were selected for repeated measurements, as well as those having altitudes approaching 130 km (127–129 km). The method for astrometric processing used in the calculations involves the use of mainly polynomial reduction models of different orders (Kozak 2002), as well as Deutsch's method at an arbitrary chosen

Downloaded from https://academic.oup.com/mnras/article/497/4/5550/5900409 by guest on 20 April 2024

optical centre (Deutsch 1965; Kozak, Rozhilo & Taranukha 2001). The original vector method was used for calculating the meteor trajectory parameters and heliocentric orbital elements (Kozak 2003). In-frame photometric measurements, which have some specific features for super-isocon TV cameras, were described in Kozak, Rozhilo & Taranukha (2001), Kozak (2014) and Kozak & Kozak (2015). Some other features of photometric processing, such as calibration, photometric correction for atmospheric absorption and calculation of the initial mass of particles are described in Kozak & Watanabe (2017). Calculation errors of kinematic meteor parameters, including errors in orbital elements, were computed using the Monte Carlo method and were described briefly in Kozak (2008). All calculations were made using the 'FALLING STAR' software (Kozak 2008), which is based on the processing methods described above.

The spatial TV system resolution was $720 \times 576 \times 8$ bit pixel^{-1}, 25 full fps at the interlaced rate. Because a meteor is a dynamical phenomenon, the use of interlaced rate cameras is complicated by the overlay of meteor images from odd and even fields (half-frames) in the full frame, shifted in time by 0.02 s. To prevent this, full frames were split programmatically into separate sequences of odd and even fields and stored in different files for further processing – the spatial resolution was reduced to 360×288. Therefore, the field of view for the Jupiter-3 lens ($f = 50$ mm, $f/1.5$) was $23.5^\circ \times 19.0^\circ$, pixel size 4 arcmin; for the Helios-40 lens ($f = 85$ mm, $f/1.5$), the field of view was $13^\circ \times 11^\circ$, the pixel size ≈ 2.2 arcmin.

Both even and odd fields were processed independently to improve the accuracy of the calculations and to detect weak images of the meteor in frames containing its possible appearance. After astrometric processing, files with the equatorial coordinates of the meteor position and corresponding time moments calculated in different fields were combined into one file. This procedure was performed for meteor images recorded at each observation station and the data obtained were subsequently used for triangulation processing. Therefore, the final temporal resolution was 0.02 s (50 fps).

2.2 The meteor of the 1993 Perseid shower

The Jupiter-3 lenses were used at both observation stations for 1991–1993 observations of the Perseid meteor shower. Among 57 meteors recorded in 1991–1993, only 46 began in the frame, which made it possible to calculate their beginning heights. Only one meteor from the 1993 Perseid shower had an extreme altitude of appearance $H_B = 136.84 \pm 0.12$ km. It should be noted that this meteor was one of the brightest in the catalogue, its absolute magnitude being $m_{\rm abs} = -3.5$ mag and its initial mass $M = 0.035$ g (two more bright meteors of absolute magnitude –3.5 and –5.0 were also detected). In all other respects, it was a usual Perseid meteor: initial velocity $\upsilon_\infty = 63.77$ km s^{-1}, heights of maximum luminosity and ending $H_{\rm MAX} = 126.80$ km and $H_{\rm E} = 105.55$ km, respectively (cosine of radiant zenith distance $\cos Z_{\rm R} = 0.715$). During observations and previous processing of the observational data, the classic physical model of the meteor dominated, according to which the beginning of meteor radiation corresponded to the beginning of intensive evaporation of the meteoroid, which, in principle, is impossible at such an altitude. Therefore, the question of the reliability of the data obtained was hotly debated. However, after numerous repeated and independent measurements, it became clear that the meteor did indeed appear at an altitude of almost 137 km and this result was first reported in Hajdukova et al. (1995); subsequently the meteor was included in the catalogue (Kruchinenko et al. 1997).

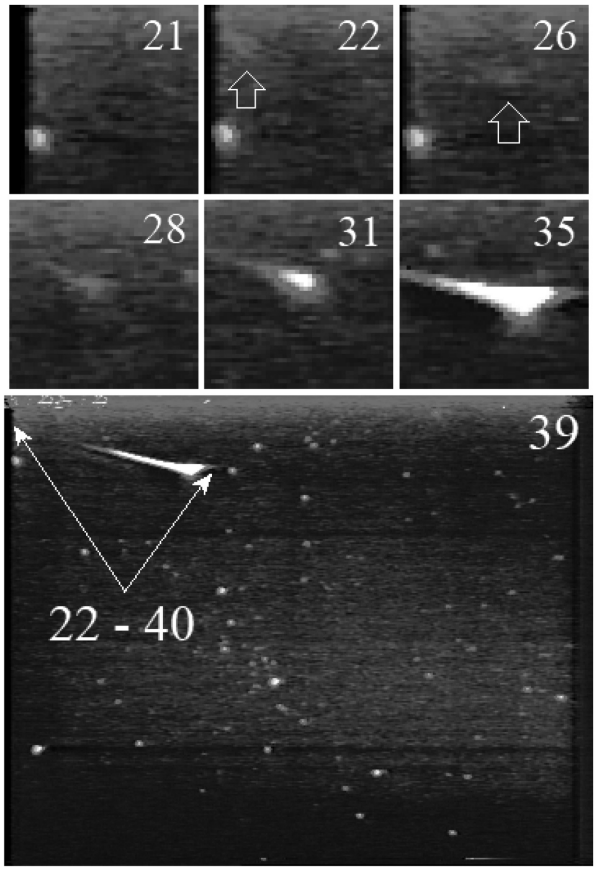

Figure 1. The meteor image detected at observation station A. The meteor develops from the 22nd to 40th half-frame (even fields of the full frame); the time interval between half-frames is 0.04 s; the 39th half-frame with the meteor image is shown completely.

2.3 The sporadic meteor in 2001

The Jupiter-3 lenses were used during September observations in 2001 and 2003. Practically all meteors were faint. Only one meteor exceeding 130 km was detected on 2001 September 22, at UT = $1^{\rm h}28^{\rm m}46^{\rm s}$. Using this meteor as an example, we will demonstrate the repeated measurements in detail, since their reliability and precision will confirm the reality of a physical phenomenon rather than artifacts of the observational equipment.

The meteor fell completely (or almost completely) inside the field of view of the camera in observation station A. It was processed in 18 odd frames and 16 even ones (34 points in total, time of flight ~0.7 s). The meteor was relatively bright at its maximum and had a prominent feature in its development. Having a classic droplet-like image in the beginning frames, the image of the meteor head (coma) transformed asymmetrically into a shape that was never observed before; see Fig. 1. As a possible explanation, we can suggest the meteor fragments into several particles, where one (or more) of them decelerated more than the others. Unfortunately, the spatial resolution of the camera does not allow us to verify or deny this.

At station B (Fig. 2), only the beginning of the meteor fell into the field of view of the camera (12 points), so this transformation of the meteor was recorded by only one station. Since, in the first frames, the meteor is extremely weak, with a signal-to-noise ratio approximately equal to one, we present in Figs 1 and 2 enlarged fragments of a meteor image in the first frames where the meteor appears and, for comparison, in some subsequent frames of the meteor development.

Downloaded from https://academic.oup.com/mnras/article/497/4/5550/5900409 by guest on 20 April 2024

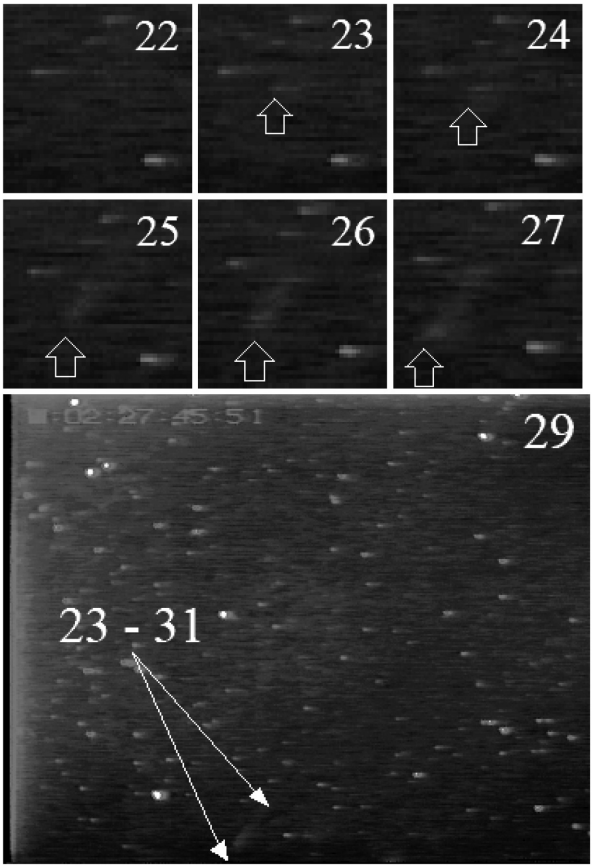

Figure 2. The meteor image detected at the observation station B. The meteor appeared in the 23rd half-frame and stayed in the field of view up to the 31st half-frame (even fields of the full frame); the time interval between the half-frames was 0.04 s; the 29th half-frame with meteor image is shown in full.

To make sure that the image in the beginning frames belongs to the meteor and not the local background elevation, we show for both observation stations the half-frames preceding the appearance of the meteor – they clearly show that any local background elevations are absent in the given places (faint images of the meteor in Figs 1–2 are shown by arrows).

At observation station A, the meteor appeared first in the 22nd half-frame (fragment 22, Fig. 1) at an altitude of 131.7 ± 0.2 km, but the frame shows that it arrived from beyond the boundary, so it could have been detected earlier. The above phenomenon of meteor coma asymmetry in the bright part of its trajectory can be seen clearly in fragment 35 and in the full 39th half-frame (Fig. 1).

As mentioned above, only the beginning of the meteor trajectory was detected at station B (Fig. 2), where its first image can be found in half-frame 23 (in the 22nd and previous half-frames, any increase of background in the potential meteor positions is missing). Calculations show the beginning height of the first meteor position as 135.1 ± 0.1 km and we assume that this is its starting altitude.

In many cases, when describing meteors with abnormally high altitudes, authors indicate only their magnitudes at maximum luminosity. However, in order to compare and evaluate such meteors recorded by different types of equipment, as well as to ensure the reliability of observational data, it is important to correlate the sensitivity of observational equipment determined by stars and

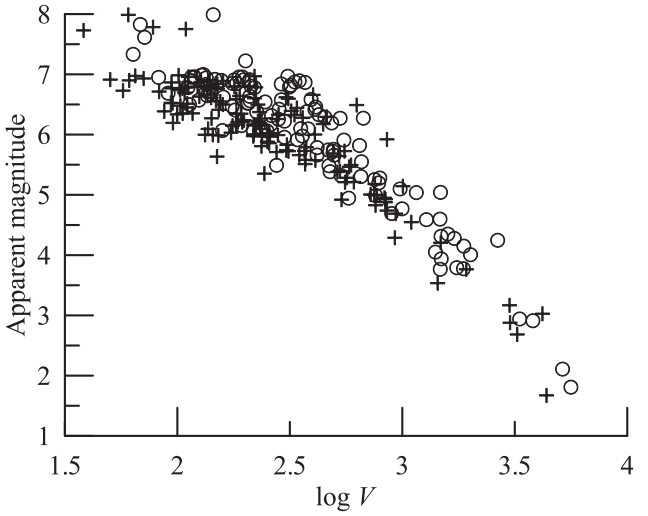

Figure 3. Calibration curves for the camera of station A (circles) and station B (pluses), where V is the photometric 'volume' of the star images measured in half-frames, i.e. the sum of intensities above the background level in all pixels belonging to the star image.

the magnitude of the meteor in the initial frames. Therefore, we present for this meteor a demonstration of its photometric processing, including the construction of calibration curves, which are indicators of the sensitivity of observational systems. The optics, sensitivity of TV transmitting tubes and weather conditions were the same for both observation stations, so the calibration curves look identical; see Fig. 3. It should be noted that the calibration curve for this type of TV transmitting tube is nonlinear. As can be seen from Fig. 3, the observation equipment sensitivity reaches, by the stars, +8 mag, so we expect that the magnitude of the meteor will be of the order of +8 mag or less (the luminosity is higher), depending on the direction of the meteor trajectory relative to the camera, on the one hand, and the focal distance of the lens, on the other. As a rule, stationary meteors are rarely observed and the difference between the meteor and the stellar limit magnitude is several units.

The meteor light curve, constructed using observational data from both observation stations, is shown in Fig. 4. In addition to the dependence of the luminosity on height, the dependence on time is also shown. The meteor flight time is 0.69 s, while the change in altitude is 46.1 km. As can be seen from Fig. 4, at the beginning of its trajectory the meteor was about +6 mag, and at maximum for 0.2 s its image was slightly supersaturated, where the magnitude was somewhat lower (the meteor was brighter) than +0.4 mag. The light curve drops sharply during about two half-frames, i.e. for a time less than 0.04 s. It is worth mentioning that the maximum magnitude was obtained by extrapolating the calibration curve slightly because of too high meteor luminosity and an absence of bright stars in the field of view.

To calculate the photometric mass of a sporadic meteor, we first calculate its light power $I_{\rm TV}$ (the energy emitted by a meteor in 1 steradian per 1 second in the wavelength band of the observational system spectral sensitivity, erg s^{-1} st^{-1}) from its out-of-atmosphere absolute magnitude (Kozak & Watanabe 2017):

$$I_{\rm TV} = 10^{0.4[C_{\rm TV} - m_{\rm abs(TV)}]+14}, \quad (1)$$

where the calibration constant of our TV photometrical system $C_{\rm TV} = -12.98$ and the term 14 is the square of the distance to the meteor in centimetres (for the absolute magnitude, obviously,

Downloaded from https://academic.oup.com/mnras/article/497/4/5550/5900409 by guest on 20 April 2024

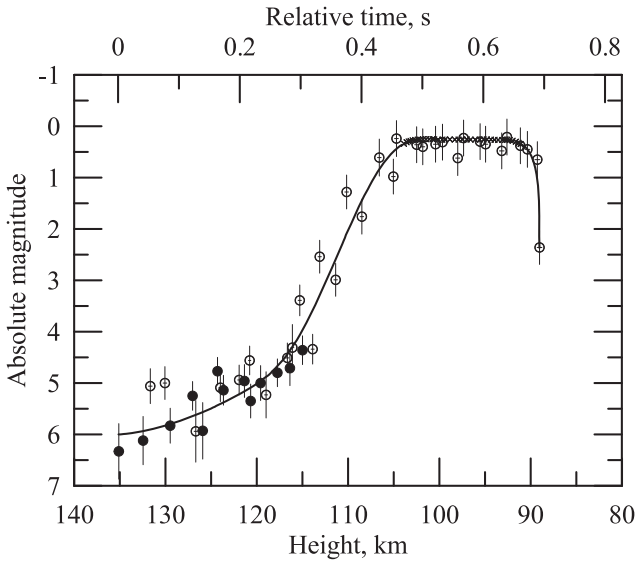

Figure 4. The meteor light curve: absolute magnitude versus altitude and time according to the observation stations A (empty circles) and B (filled circles). The errors correspond to one standard deviation; the beginning of the time-scale corresponds to the first moment of the meteor's appearance (at station B). The solid line is a polynomial approximation. The supersaturated region of the light curve is drawn with the dotted line.

it is 100 km). Next, we use the classic formula for the meteor light power, which is proportional to the rate of meteoroid kinetic energy loss (deceleration neglected):

$$4\pi I_{\rm TV}(t) = -\tau \frac{\upsilon^2}{2} \frac{{\rm d}M}{{\rm d}t}, \qquad (2)$$

where the radiation efficiency coefficient τ is established similarly to Campbell-Brown & Koschny (2004): $\tau \approx 2 \times 10^{-3}$ (similar values are presented in the books by Levin 1956 and Bronshten 1983, for example).

Then the initial mass of the meteoroid M_0 can be found by integrating the formula (2) over the time of flight: it was found to be $M_0 \approx 0.04$ g. We consider this meteor to be a sporadic one, with velocity $\upsilon_{\rm G} = 67..8 \pm 0.4$ km s^{-1}, equatorial coordinates of geocentric radiant $\alpha_{\rm G} = 59.87^\circ \pm 0.04^\circ$, $\delta_{\rm G} = 27.77^\circ \pm 0.11^\circ$ and ecliptic longitude of the Sun $\lambda_{\rm SOL} \approx 178.8^\circ$. The closest in kinematic parameters to it is the September ξ- Perseids (SXP) shower (Jopek & Kaňuchová 2017): $\upsilon_{\rm G} = 66.5$ km s^{-1}, $\alpha_{\rm G} = 59.8^\circ$, $\delta_{\rm G} = 37.9^\circ$, $\lambda_{\rm SOL} \approx 174.8^\circ$, but as is seen, the declination differs by 10°.

2.4 The meteors of the 2002 Leonid shower

During observations of the theoretically predicted meteor storm of Leonids in 2002, we registered 38 double-station meteors; 28 of them were included in the catalogue (Kozak et al. 2007). The conditions of observations were extremely unfavourable – there was a bright moon about 30° above the horizon, while the shower radiant was in the field of view of one camera – so processing was reduced mainly to calculating the radiant and orbital elements of the meteoroid cluster. All meteors at the maximum were too bright for correct determination of their magnitude, so the calibration curve was extrapolated. However, several meteors with altitudes above 130 km and several with altitudes of about 128–129 km were recorded. In total, six meteors were selected and reprocessed together in even and odd half-frames in a way similar to the sporadic meteor processing. It should be noted that, at observation station A, the same lens Jupiter-3 ($f = 50$ mm, $f/1.5$) was used and at station B a longer focus distance (and larger aperture) lens Helios-40 ($f = 85$ mm, $f/1.5$) was used. Therefore, the calibration curve constructed for the stars at observation station A was limited by +8 mag, and at station B the maximum stellar magnitude was +9 mag. Thus, for the five meteors, the following pairs of approximate values of beginning heights of meteors at stations A and B were obtained: (>124 km; 143 km), (131 km; 135 km), (127 km; 144 km), (131 km; 140 km), (128 km; 138 km). More precise values of the meteor parameters are given in Tables 1 and 2. The values of meteor magnitude at the beginning heights have large errors because of a low signal-to-noise ratio caused by the bright moon, but on average they lie in the range +5.5 to +6.5 mag. Of interest is the sixth meteor processing result – its altitude at station B was calculated as almost 170 km, while being recorded as only 121 km at observation station B. After the analysis, we found that the angle between the meteor's trajectory and the direction to observation station B varied between 2.8° and 4.5° (the meteor was almost stationary), which indicates an extremely rough determination of the meteor radiant, so it was excluded from further consideration. However, these data demonstrate one of the possible causes of incorrect determination of meteor heights, which should be taken into account in the future.

The fact that the meteors belonged to one compact cluster of the meteor stream and were observed almost simultaneously, all had the same angles of entry into atmosphere (the zenith distance of the radiant was near 28°–29°, except one case with $Z_{\rm R} \approx 43^\circ$) and had almost the same initial masses accounts for almost identical view of their light curves shown in Fig. 5. The light curves were plotted using the observation results obtained at station A, because at observation station B the images of all meteors were very supersaturated, so the beginnings of the light curves in Fig. 5 lie in the range 123–131 km.

Table 1. Kinematic parameters of meteor detection at the observation stations. Indices 'b' and 'e' denote the beginning and end of meteor detection; 'H' is the altitude; 'γ' is the angle between the meteor velocity vector and the direction to the observation station.

No	Meteor registration Date UT	Time	Detection (A) $H_{\rm b}$ (km)	$H_{\rm e}$ (km)	$\gamma_{\rm b}$ (°)	$\gamma_{\rm e}$ (°)	Detection (B) $H_{\rm b}$ (km)	$H_{\rm e}$ (km)	$\gamma_{\rm b}$ (°)	$\gamma_{\rm e}$ (°)
Per 1	1993–08-12	20:19:44	–	–	–	–	136.8 ± 0.1	105.6 ± 0.1		
Spo 1	2001–09-22	01:28:46	$> 131.7 \pm 0.2$	89.0 ± 0.3	12.6	18.8	135.1 ± 0.1	$<119.6 \pm 0.2$	15.4	17.3
Leo 1	2002–11-19	01:36:34	$> 123.8 \pm 0.2$	97.2 ± 0.1	35.7	48.4	133.8 ± 0.3	97.0 ± 0.1	13.0	19.1
Leo 2	2002–11-19	03:53:23	131.2 ± 0.1	92.1 ± 0.1	20.3	30.0	134.5 ± 0.2	91.3 ± 0.1	14.6	21.3
Leo 3	2002–11-19	03:54:17	127.0 ± 0.1	$< 98.3 \pm 0.6$	30.4	40.1	144.3 ± 0.1	$<104.2 \pm 0.2$	17.0	23.9
Leo 4	2002–11-19	04:05:50	131.2 ± 0.2	92.6 ± 0.6	19.3	28.2	140.3 ± 0.1	90.5 ± 0.1	15.2	23.2
Leo 5	2002–11-19	04:05:54	127.8 ± 0.1	$< 94.9 \pm 0.1$	27.9	38.4	137.9 ± 0.1	$<100.3 \pm 0.1$	19.1	26.3

Downloaded from https://academic.oup.com/mnras/article/497/4/5550/5900409 by guest on 20 April 2024

Table 2. Common parameters of meteors with extreme beginning heights. Abbreviations: Δt = time of existence; index R = radiant; index G = geocentric; MAX = maximum of brightness; Z = zenith distance (of radiant); M = mass. The other abbreviations are standard or analogous to Table 1.

No	Δt s	α_{RG} (°)	δ_{RG} (°)	υ_G (km s^{-1})	υ_∞ (km s^{-1})	Z_{Rb} (°)	H_{MAX} (km)	m_{MAX} ()	M (g)
Per 1	–	47.69 ± 1.30	58.08 ± 1.30	62.6	63.8	44.4	126.8	–3.50	0.35
Spo 1	0.69	59.87 ± 0.04	27.77 ± 0.11	67.8	68.7	22.5	97.2	<+0.21	0.04
Leo 1	0.53	154.35 ± 0.09	21.31 ± 0.08	71.3	72.1	43.3	107.6	− 0.08	0.03
Leo 2	0.56	154.84 ± 0.03	21.80 ± 0.04	75.1	75.9	28.7	104.6	− 0.15	0.03
Leo 3	0.40	154.80 ± 0.03	21.25 ± 0.04	72.8	73.6	29.3	108.2	− 0.64	0.05
Leo 4	0.60	154.66 ± 0.02	21.75 ± 0.01	71.9	72.7	28.2	114.2	0.06	0.03
Leo 5	0.48	154.31 ± 0.01	21.98 ± 0.01	73.4	74.3	28.2	105.9	− 0.53	0.06

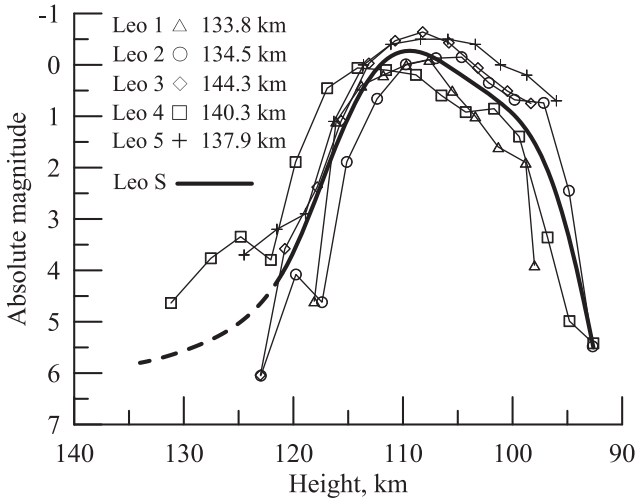

Figure 5. Light curves of the five Leonids obtained at observation station A and their averaged synthetic light curve. Values of the beginning heights for the corresponding meteors at observation station B are also shown in the figure, see the description in Tables 1–2.

The values of the corresponding higher beginnings of the meteors detected at observation station B with the camera of larger aperture are also shown in the figure. As one can see from Fig. 5, all meteors start and disappear smoothly (unlike the sporadic meteor shown in Fig. 4, which disappears almost instantly) within about +6 to +5 mag, having almost the same gradients of light curves. The only Leo 4 meteor light curve, which has an inflated value of meteor luminosity in a few initial frames, was measured with large errors. The conformity of the given light curves makes it possible to construct for further analysis a certain averaged synthetic light curve of a hypothetical meteor (designated here as Leo S), shown in Fig. 5 with a bold line. A distinctive feature of all the light curves of this Leonid meteor cluster is their asymmetric shape immediately before and after maximum. Immediately after maximum, the gradient of the light curve has the same value as before it, followed by a significant decrease; then, before complete particle disintegration, the curve increases sharply again. This feature of the light curves of the aforementioned Leonid filament can be used in future for analysis of the ablation process.

3 DISCUSSION

The generalized results of the refined processing of the meteors, including additional kinematic and photometric parameters, on which the accuracy of calculation of a meteor trajectory potentially depends, are summarized in Table 1. As can be seen from the table, the sporadic meteor and two meteors belonging to the Leonid shower have beginning heights above 130 km at both observational stations, which corroborates the results' reliability. As noted earlier, an important parameter to be monitored when processing meteor observations is the angle between the meteor velocity vector and the direction to the observation station, as it can lead to rough errors in determining radiant coordinates and, consequently, erroneous altitudes. As can be seen from Table 1 for the Leonid shower meteors, the angle mentioned was in the range ∼25° to 50° for observation station A and ∼15° to 25° for station B. These values are not optimal for very good accuracy, but sufficient for correct calculations.

Some additional kinematic and photometric parameters of the meteors are shown in Table 2. As evident from the table and as mentioned above, meteors of the 2002 Leonid storm compact cluster had similar zenith angles of the radiant (except Leo1), similar velocities and close initial masses, so they have similar values of magnitudes in their maximum brightness – near 0 mag (let us recall that these values were obtained by a small extrapolation of the calibration curve and meteors could be slightly brighter). The Leonid meteor images being oversaturated, the meteor head coordinates in each frame were not measured very precisely, so their velocities have an error (standard deviation) of about 1–2 km s^{-1}.

The reliability of meteor beginning height calculations depends, first of all, on the precision of astrometric processing of meteor images in the initial frames. The astrometric calculation precision, in its turn, depends on a sufficient number of comparison stars and a correctly selected reduction model, which would take into account geometric and photometric distortion in TV frames. In the case of our observations, the accuracy of the calculations was given special attention and the presence of meteors with altitudes of 130–145 km can be assured.

If we accept the hypothesis of meteor radiation at ultrahigh altitudes, which assumes that the mechanism of radiation is not associated with evaporation or melting of meteoroids, but is due only to direct collisions of the meteoroid surface with air molecules (sputtering), according to e.g. Popova, Strelkov & Sidneva (2007), it can be assumed that a meteor begins to emit 'from infinity'. In this case, the probability of detection is associated only with the intensity of the meteor radiation and the sensitivity of the observation equipment. When observing this Leonid cluster, we did not register extremely high altitudes of more than 145 km, on the one hand, but, on the other hand, we did not register bright fireballs that could create sufficiently intense radiation at such altitudes either.

Analysing the light curve of the sporadic meteor in Fig. 4, it is logical to assume that its upper flat segment of approximately zero magnitude, in accordance with classic meteor physics, corresponds to boiling and intensive evaporation of the body, accompanied by

Downloaded from https://academic.oup.com/mnras/article/497/4/5550/5900409 by guest on 20 April 2024

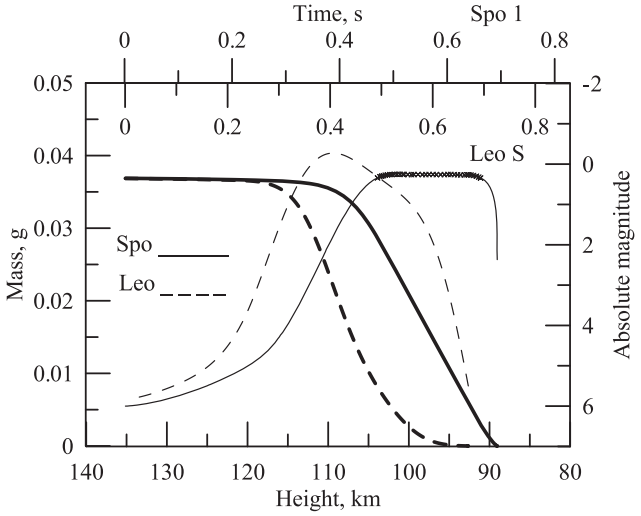

Figure 6. Mass loss by sporadic meteoroid Spo 1 and averaged synthetic 'meteor' Leo S from the 2002 Leonid stream (left *y*-axis) as a function of altitude and time. For comparison, the corresponding light curves of the meteors from Figs 4–5 are shown (right *y*-axis; the values on the left and right *y*-axes are not related directly).

rapid ablation (mass loss) of the particle. Using formulae (1) and (2), we can plot a curve of the mass loss versus time and height for the sporadic meteor. This curve is presented in Fig. 6: it demonstrates a residual mass of the sporadic meteoroid along its path in atmosphere (the altitude change being 46.1 km), within the time range of 0.69 s. According to the curve, from altitudes of 135–115 km, i.e. for 20 km of altitude change, the meteor lost only 1 per cent of its mass (the speed of mass loss was 10^{-4}–10^{-3} g s^{-1}). Then, probably, a transitional period of increasing the meteor radiation intensity and the rate of mass loss (assuming the radiation efficiency coefficient remained unchanged) began, where, at an altitude of 110 km, the meteor lost more than 3 per cent of its mass ($\mathrm{d}M/\mathrm{d}t \approx 0.02\,\mathrm{g\,s^{-1}}$) and reached maximum luminosity at an altitude of about 106 km, having lost 12 per cent of its initial mass before that. The rate of mass loss at the maximum was almost 0.14 g s^{-1}.

A similar curve can be plotted for the synthetic meteor of the 2002 Leonid shower, conditionally extending the beginning of its light curve to the altitude of the sporadic meteor, 135.1 km, using to that end some averaged parameters such as $\bar{Z}_\mathrm{R} \approx 28.6^\circ$, $\bar{v}_\infty \approx 72.4$ km s^{-1} (inflated hyperbolic values of meteor velocities from Table 2 were excluded from averaging as erroneous). It is noteworthy that the initial mass of this synthetic Leonid meteor coincides with the mass of the sporadic meteor up to three decimal digits and also amounts to 0.037 g. The curve of mass loss for the Leonid synthetic meteor is shown in Fig. 6 with a dashed line: during 0.67 s it passed the distance of 48.4 km, changing its altitude for 42.5 km. Due to the higher velocity and, probably, lower density, heating and ablation processes occurred faster in comparison with the sporadic meteor. At an altitude of 119 km, the meteor had already lost the first per cent of its mass, at 116.5 km it had lost 3 per cent and intense mass loss began somewhere around an altitude of 112 km, where the meteoroid lost 19 per cent of its initial mass. The rate of mass loss in the respective sections of the trajectory was 5.8×10^{-3}, 0.03 and 0.2 g s^{-1}, respectively.

It would be highly desirable to associate different parts of the sporadic meteor light curves, as well as those from the Leonid shower, especially at the beginning of their trajectories, with the corresponding physical processes: energy exchange of a space particle with atmosphere molecules without mass loss; cold sputtering of the meteoroid's surface layer; blowing the molten layer off; intensive evaporation of the body. Building a complete model of the meteoroid's motion in the atmosphere, taking into account deceleration, heating and ablation, to describe an individual meteor's light curve in detail presents a challenge that goes beyond the scope of this work. However, it is possible to carry out a qualitative analysis of meteor light curves in relation to the changing the meteoroid temperature, which depends on the altitude, using a somewhat simplified approach. To do this, we first consider the classic equation of energy balance at the stage of meteoroid heating (Levin 1956; Bronshten 1983):

$$S_\mathrm{M}\frac{\Lambda v_0^3}{2}\rho_\mathrm{a}(t) = c_\mathrm{p}M_0\frac{\mathrm{d}T(t)}{\mathrm{d}t} + S_\mathrm{F}\varepsilon\sigma\left[T(t)^4 - T_0^4\right], \quad (3)$$

where S_M and S_F are the the areas of the cross-section and the entire surface of the space particle, respectively (for a spherical particle it is obvious that $S_\mathrm{F} = 4S_\mathrm{M}$); v_0 and M_0 are the initial velocity (deceleration neglected) and mass of the meteoroid; $T(t)$ and T_0 are the temperature of the whole body for isothermal heat distribution and equilibrium temperature in the given part of the atmosphere; $\rho_\mathrm{a}(t)$ is the atmosphere density; Λ is the energy transfer coefficient; c_p is the specific heat capacity of the substance; $\varepsilon \approx 0.9$ is the emissivity of the meteoroid. To simulate the heating of the sporadic meteor, let us consider four possible variants of a stone with densities of 1.0, 1.5, 2.5 and 3.5 g cm^{-3}, as well as an iron body with a density of 7.85 g cm^{-3}. The melting and boiling temperature will be assumed to be 1690 and 2100 K, respectively (for iron, 1810 and 3135 K, according to Desai 1986). Calculated in accordance with (3), the heights of the beginning of fusion and evaporation for the spherical sporadic meteoroid were $H_\mathrm{melt} \approx 106$ km, $H_\mathrm{boil} \approx 100$ km; $H_\mathrm{melt} \approx 103$ km, $H_\mathrm{boil} \approx 97$ km; $H_\mathrm{melt} \approx 101$ km, $H_\mathrm{boil} \approx 95$ km; and $H_\mathrm{melt} \approx 100$ km, $H_\mathrm{boil} \approx 94$ km for densities 1, 1.5, 2.5 and 3.5 g cm^{-3}, respectively. In the case of the iron particle, the corresponding heights are 98 and 92 km. Comparing the obtained pairs of temperature values with the meteor light curve (Figs 4 and 6), we can conclude that the stone particle is much better suited to the role of this meteoroid than the iron one. Nevertheless, to be sure, it is also important to estimate the magnitude of the meteor along the trajectory and compare it with the real light curve. To construct the calculated meteor light curve, we will continue to apply a simplified approach using an isothermal body and use the ablation equation (Levin 1956; Bronshten 1983), similar to equation (3), where the heating process after reaching the appropriate temperature is replaced by a phase transition, i.e. melting and then evaporation:

$$S_\mathrm{M}\frac{\Lambda v_0^3}{2}\rho_\mathrm{a}(t) = -Q\frac{\mathrm{d}M(t)}{\mathrm{d}t} + S_\mathrm{F}\varepsilon\sigma\left[T(t)^4 - T_0^4\right], \quad (4)$$

where Q is the heat of evaporation of the body. The calculated meteor light curves, which describe the process of particle evaporation directly, are shown in Fig. 7; there are also melting points for meteoroids of different densities. In general, given the fact that the image of the real meteor was somewhat supersaturated at its maximum luminosity segment, the calculated light curves for the stone particles describe the change in luminosity of the meteor adequately at its maximum and in its final segment. Meanwhile, the iron body model cannot correctly explain the radiation of the given particle. As can be seen from Fig. 7, a stone particle with a density of about 2 g cm^{-3} describes the meteor light curve best. However, it should be noted that the calculated light curves are closely related to the chosen melting and evaporation temperatures. If, in Fig. 7,

Downloaded from https://academic.oup.com/mnras/article/497/4/5550/5900409 by guest on 20 April 2024

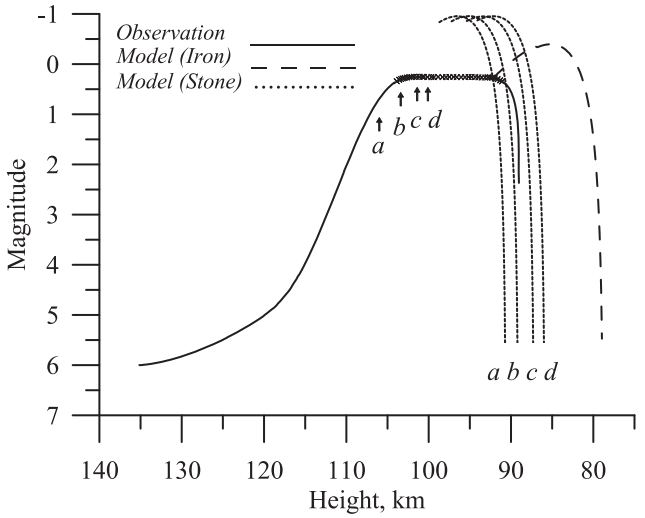

Figure 7. Modelling the light curves of the sporadic meteor Spo 1 as an isothermal stone body of different densities: (a) $\rho = 1$ g cm^{-3}, (b) $\rho = 1.5$ g cm^{-3}, (c) $\rho = 2.5$ g cm^{-3} and (d) $\rho = 3.5$ g cm^{-3} (dotted lines); and an iron body with a density of 7.85 g cm^{-3} (dashed line). The solid line is the original light curve from observations (Fig. 4). The arrows at the bottom of the curve indicate the heights of the corresponding melting temperatures.

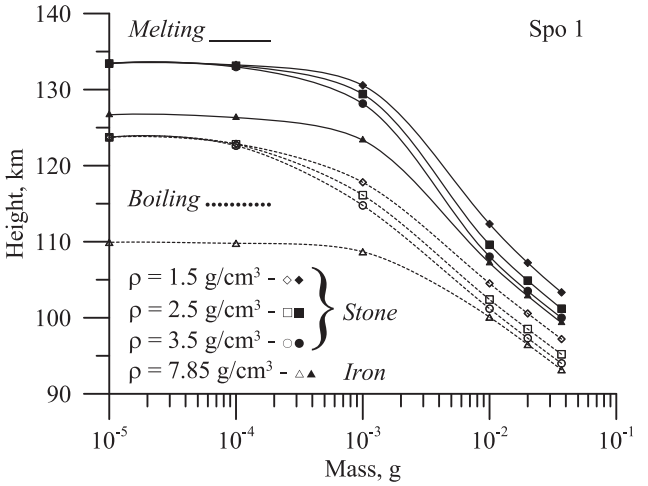

Figure 8. Dependence of the height of meteor melting and evaporation beginning on the mass of a cylindrical meteoroid with a constant cross-section. The curves are constructed for the sporadic meteor (kinematic parameters are presented in Table 2).

the mentioned temperatures increase, all the calculated light curves will shift to the right and the best candidate for the description of this meteor will be the particle with a density of 1–1.5 g cm^{-3}; if the melting and evaporation temperatures are lower than the selected ones, the meteor is best described by the particle with a density of about 3.5 g cm^{-3}.

Our chosen simplified isothermal model links the beginning of meteor radiation to the start of meteoroid evaporation, ignoring other processes such as melting, and does not describe the first segment of the light curve, especially the beginning of radiation.

Obviously, the cause lies in the large mass of the meteoroid, which corresponds to a body size 2–3 mm, i.e. slightly bigger than the depth of uniform heating according to Levin (1956), and, consequently, the body cannot be supposed to be isothermal. Probably, in this case it is possible to apply the approach in which we consider that at first only part of the body warms up to the melting and then evaporation temperature. The rate and depth of heating of such a frontal part of the body depends (in addition to the velocity of the space particle and its angle of entry into the atmosphere) on the temperature conductivity coefficient. Thus, if we neglect, at the stage of meteoroid heating, heat transfer into the body beyond the selected depth, we will obtain the upper limit of heights of meteor melting and evaporation beginning, which could explain the high altitudes of such relatively low-mass meteoroids. To find the beginning heights of melting and evaporation, we will again use equation (3). For convenience, we will use a cylinder body shape moving with the base ahead. The initial cross-section values (the area of the cylinder bases) for stone particles of different densities will be chosen equal to the corresponding cross-sections of a spherical particle of diameter d, which corresponds to an initial mass of the sporadic meteoroid 0.037 g; then the initial ratio of heating depth h to d will be $h/d \approx 0.67$. Next, at each step of the calculations we will reduce the mass of the heated zone and, accordingly, the depth of heating by an order, to a certain minimum value. At this stage, the discrepancy in the values of the heated mass of the body and its integral mass does not play any role, because we neglect the deceleration of the particle and, accordingly, do not consider the equation of motion where the mass of the whole body is present.

The melting and evaporation beginning heights of this sporadic meteor of stone and iron substance, depending on the heated area mass of the meteoroid, are given in Fig. 8. The rightmost values in the figure correspond to the integral mass of the particle $M = 0.037$ g. As can be seen from the figure, for the heated zone of meteoroids, starting from a mass of about 10^{-4}, the beginning height of melting and evaporation does not depend on the density of the stone particle and constitutes respectively $H_{\rm melt} \approx 133.4$ km and $H_{\rm boil} \approx 123.7$ km. For the iron particle, the given values differ because of the lower energy transfer coefficient (we assume the value $\Lambda = 0.75$ for iron, while $\Lambda = 1$ for stone: Levin 1956) and constitute respectively $H_{\rm melt} \approx 126.7$ km and $H_{\rm boil} \approx 109.9$ km. This asymptotic region of initial melting and evaporation heights corresponds to the case of Whipple's micrometeorite theory (Whipple, 1950, 1951), where the first item on the right-hand part of equation (3) can be neglected due to its small contribution to the energy balance equation (Öpik, 1937). Using the equation of ablation (4), we can show that the mass of 10^{-4} g for the kinematic parameters of this meteoroid provides an initial value of the meteor magnitude of +5 to +6 mag, i.e. corresponds to the detection limit of our observational equipment. Thus, the maximum beginning height of this sporadic meteor with mass of 0.037 g due to the melting of its surface will be provided at a heating depth of at least $h \leq 5 \times 10^{-4}$ cm, which is approximately 0.3 per cent of the initial total mass of this particle.

The subsequent process of ablation can occur in different ways, e.g. by blowing the surface of the meteoroid in the form of droplets: such a model was developed for weak slow (15–25 km s^{-1}) iron meteoroids observed at altitudes of 80–90 km (Čapek & Borovička 2017; Čapek et al. 2019). The model provides different average sizes of liquid droplets from several to several hundred micrometres, which in principle does not contradict the minimum heating depth of 5 μm obtained here.

The analysis of the curves in Fig. 8 also clearly shows that the sporadic meteoroid could not be an iron one, as it appeared well above the altitude of the calculated beginning of iron particle melting, $H_{\rm melt} \approx 126.7$ km. Moreover, the observation results presented in Čapek et al. (2019) show that iron particles create a very specific

Downloaded from https://academic.oup.com/mnras/article/497/4/5550/5900409 by guest on 20 April 2024

type of light curve, where the luminosity increases sharply at the initial part of the trajectory, while we have an opposite situation. Meanwhile, the stone particles correspond to the ablation process calculation results very well, providing the meteor magnitude is +6 to +5.5 mag at the evaporation beginning height of 124 km, which is in good agreement with the light curve of the sporadic meteor. At the same time, the beginning part of the light curve falls in the altitude range where the frontal part of the particle has already been melted (under 133 km) and probably corresponds to the process of blowing the molten layer off from the meteoroid surface.

Similar calculations can be performed for the meteor Leo S, assuming the density of Leonid shower meteoroids is 1 g cm^{-3} (Jenniskens 2006, Borovicka 2007). The beginning heights of melting and intense evaporation of Leonids are $H_{\rm melt} \approx 136.3$ km and $H_{\rm boil} \approx 125.1$ km for the heated frontal zone mass 10^{-4} g. This melting height corresponds well to the limiting sensitivity of the observational equipment and meteor beginning heights and gives values of +6 to +5 mag. However, three meteors from the Leonid shower with beginning heights of 138–144 km become visible even before the melting height of the meteoroids; probably the reason for their radiation at these altitudes is surface sputtering (Popova, Strelkov & Sidneva 2007) or energy exchange with atmosphere molecules and atoms without mass loss. The latter assumption is partly corroborated by the results of Spurný et al. (2014), where bolide spectral analysis showed the presence of only atmosphere emission at extreme altitudes. On the other hand, such heights could also be explained by the blowing off of the molten layer of the meteoroid surface assuming a lower temperature of melting. Thus, at a melting point of about 1600 K the altitude will be about 140 km, and at 1500 K it will be 145 km. If we assume that the melting temperatures of these Leonid stream meteoroids can vary in the range 1500–1700 K due to their composite structure, the need to attract the model of 'cold' surface sputtering will disappear.

4 CONCLUSIONS

All cases of meteor detection described here at altitudes above 130 km belong to fast meteors in the range 63–72 km s^{-1}, as in most cases described by other authors (with the exception of one Lyrid having a velocity of 45.3 km s^{-1}, described in Koten et al. 2001). However, the peculiarity of these meteors is their relatively small mass of 0.03–0.06 g and, correspondingly, low luminosity of the order of 0 mag (the exception is the less fast Perseid, with a velocity of 62.6 km s^{-1}, –3.5 mag and mass one order greater, 0.35 g). The very specific shape and features of the sporadic meteor light curve are noteworthy and still need to be explained. Another interesting observation is the light-curve asymmetry and gradient change immediately after maximum in all five Leonids belonging to the same compact cluster of this 2002 meteor stream. The ratios of sporadic meteor mass loss of 0.14 g s^{-1} and 0.20 g s^{-1} for the Leonids at their maximum luminosity and about 10^{-3} g s^{-1} at the beginning of the trajectory are almost the same for all meteors, which is attributed to their close velocity values. The assumption that a meteor may be detected when its surface has melted to a certain depth generally describes all the characteristics of the light curves of these meteors: they were stone meteors and for them, at the beginning of the trajectory, the depth of heating was about 10^{-4} cm, with a corresponding mass of 10^{-4} g (0.3 per cent of the initial total mass). Furthermore, as shown, these values do not depend on the density of the meteoroid substance (for fixed energy transfer coefficient Λ). These values also provide a magnitude of +6 mag at the beginning of detection, which agrees well with the sensitivity of the observation equipment. However, these results were obtained from calculations where the melting point of the body was about 1690 K, which is typical for silicon, whereas some authors take slightly higher values, such as 1900 K (Campbell-Brown & Koschny, 2004). In addition, the height of meteors 140–145 km can be explained only by reducing the melting temperature to 1600–1500 K, otherwise we should assume that the meteors appear not because of the molten layer blowing off but due to sputtering of the 'cold' surface of the meteoroid. While taking all these data into account, as well as neglecting heat transfer deep into the space particle in the calculations, we cannot state unambiguously that the detection of these space particles began at the time when the already molten layer was being blown off the surface. This demonstrates that such a model is possible in principle, thus making non-essential a referral to a model of 'cold' sputtering of the meteoroid surface.

ACKNOWLEDGEMENTS

Part of this work was achieved using the grant of the Visiting Scholar Program supported by the Research Coordination Committee, National Astronomical Observatory of Japan (NAOJ).

DATA AVAILABILITY

The data underlying this article are available in the article and in its online supplementary material.

REFERENCES

Abe S., Borovička J., Spurný P., Koten P., Ceplecha Z., Tamagawa T., Meteor Network Team in Japan, 2006, Structuring the European Research Area – Research Infrastructures Action. Abs. European Plan. Sci. Cong., Berlin, p. 486
Betlem H. et al., 1999, Meteoritics and Planetary Science, 34, 979
Borovička J., Ceplecha Z., 1992, A&A, 257, 323
Borovička J., 2007, in Milani A., Valsecchi G. B., Vokrouhlick´y D., eds, Proc. IAU Symp. 236, Near Earth Objects, our Celestial Neighbors: Opportunity and Risk, Cambridge University Press,p. 107
Bronshten V. A., 1983, The Physics of Meteoritic Phenomena. D. Reidel Publishing Co., Dordrecht
Campbell M. D., Brown P.G., LeBlanc A.G., Hawkes R., Jones J., Worden S., Correll R., 2000, Meteoritics and Planetary Science, 35, 1259
Campbell-Brown M.D., Koschny D., 2004, A&A, 418, 751
Čapek D., Borovička J. 2017, Planet. Space Sci., 143, 159
Čapek D., Koten P., Borovička J., Vojáčk V., Spurný P., Štork R. 2019, A&A, 625, A106
Ceplecha Z., 1994, A&A, 283, 287
Desai P. D., 1986, J. Phys. Chem. Ref. Data, 15,, Near Earth Objects, our Celestial Neighbors: Opportunity and Risk967
Deutsch A. N., 1965, Astron. Zh., 42, 1144
Fujiwara Y., Ueda M., Shiba Y., Sugimoto M., Kinoshita M., Shimoda C., Nakamura T., 1998, Geophys. Res. Lett., 25, 285
Gährken B., Michelberger J., 2003, WGN, the Journal of the IMO, 31, 137
Hajdukova M., Kruchinenko V. G., Kazantsev A. M., Taranucha Ju.G., Rozhilo A. A., Eryomin S. S., Kozak P. N., 1995, Earth, Moon and Planets, 68, 297
Jenniskens P., 2006, Meteor Showers and their Parent Comets. Cambridge University Press, Cambridge, UK, p. 804
Jopek T., Kaňuchová Z., 2017, Planet. Space Sci., 143, 3
Kinoshita M., Maruyama T., Sagayama T., 1999, Geophys. Res. Lett., 26, 41
Koten P., Spurný P., Borovička J., Štork R., 2001, in Warmbein B., ed, ESA SP-495, Extreme beginning heights for non-Leonid meteors, ESA Publications Division, Noordwijk,p. 119
Koten P., Čapek D., Spurný P., Vaubaillon J., Popek M., Shrbený L. 2017, A&A, 600, A74

Downloaded from https://academic.oup.com/mnras/article/497/4/5550/5900409 by guest on 20 April 2024

Koten P., Rentdel J., Shrbený L., Gural P., Borovička J., Kozak P., 2019, in Ryabova G.O., Asher D.J., Campbell-Brown M.D., eds, Sources of Meteors on Earth and Beyond. Cambridge University Press, Cambridge, p. 90
Kozak P. M., 2002, Kinem. Phys. Celest. Bodies, 18, 471
Kozak P. M., 2003, Kinem. Phys. Celest. Bodies, 19, 62
Kozak P. M., Rozhilo A. A., Taranukha Y. G., 2001, in Warmbein B., ed, ESA SP-495, Some features of digital kinematic and photometrical processing of faint TV meteors, ESA Publications Division, Noordwijk, p. 337
Kozak P., Rozhilo O., Kruchynenko V., Kazantsev A., Taranukha A., 2007, Adv. Space Res., 39, 619
Kozak P., 2008, Earth, Moon, and Planets, 102, 277
Kozak P., Rozhilo O., Taranukha Ju., Kruchynenko V.G., 2011, Space Sci. Technol., 17, 51
Kozak P., Rozhilo O., Taranukha Ju., 2012, Bulletin of Taras Shevchenko National University of Kyiv. Astronomy, 49, 20
Kozak P. M., 2014, in Jopek T.J., Rietmeijer F.J.M., Watanabe J., Williams I.P., eds, A.M. Univ. Press, Poznań, p. 335
Kozak P., Watanabe J., Sato M., 2014, in Muinonen K., Penttila A., Granvik M., Virkki A., Fedorets G., Wilkman O., Kohout T., eds, Abs. Book ACM'2014, p. 310
Kozak P. M., Kozak L.V., 2015, Space Sci. Technol., 21, 38
Kozak P. M., Watanabe J., 2017, MNRAS, 467, 793
Kozak P., 2017, Bulletin of Taras Shevchenko National University of Kyiv Astronomy, 56, 6
Kozak P. M., 2019, Kinem. Phys. Celest. Bodies, 35, 286
Kruchinenko V. G, Kazantsev A. M., Taranukha Yu.G., Kozak P. M., Yeryomin S. S., Rozhylo O. O., Smertyuk L. M., 1997, Bulletin of Taras Shevchenko National University of Kyiv. Astronomy, 34, 94
LeBlanc A. G. et al., 2000, MNRAS, 313, L9
Levin B. Y., 1956, Physical Theory of Meteors and Meteor Matter in the Solar System. USSR Academy of Sciences, Moscow
Madiedo J. M., Espartero F., Castro-Tirado A. J., Pastor S., de los Reyes J. A., Jose A., 2016, MNRAS, 460, 917
Öpik E., 1937, Publ. Tartu Astrofizica Observatory, 29, 1
Olech A. et al., 2013, A&A, 557, A89
Popova O. P., Strelkov A. S., Sidneva S. N., 2007, Adv. Space Res., 39, 567
Roberts I. D., Hawkes R. L., Weryk R. J., Campbell-Brown M.D., Brown P.G., Stokan E., Subasinghe D., 2014, in Jopek T. J., Rietmeijer F. J. M., Watanabe J., Williams I .P., eds. A. M. Univ. Press, Poznań, p. 155
Spurný P., Betlem H., Jobse K., Koten P., Leven J. V., 2000a, Meteoritics and Planetary Science, 35, 1109
Spurný P., Betlem H., Leven J.V., Jenniskens P., 2000b, Meteoritics and Planetary Science, 35, 243
Spurný P., Shrbený L., Borovička J., Koten P., Vojáček V., Štork R., 2014, A&A, 563, A64.
Stenbaek-Nielsen H.C., Jenniskens P., 2004, Adv. Space Res., 33. 1459
Taylor M. J., Gardner R. C., Murray I. S., Jenniskens P., 2000, Earth, Moon and Planets, 82–83, 379
Watanabe J., Tabe I., Hasegawa H., Hashimoto T., Fuse T., Yoshikawa M., Abe S., Suzuki B., 2003, PASJ, 55, L23
Whipple F. L., 1950, Proc. Nat. Acad. Sci. Amer., 36, 687
Whipple F. L., 1951, Proc. Nat. Acad. Sci. Amer., 37, 19

This paper has been typeset from a TEX/LATEX file prepared by the author.

Downloaded from https://academic.oup.com/mnras/article/497/4/5550/5900409 by guest on 20 April 2024